HiSST: 3rd International Conference on
High-Speed Vehicle Science Technology
14 -19 April 2024, Busan, Korea

Experimental Investigation of Film Cooling Effectiveness Using Different Coolant Gases in Hypersonic Flows

Jithin Sreekumar[1], Talluri Vamsi Krishna[2], Honhar Gupta[3],Mohammed Ibrahim Sugarno[4]

Abstract

An experimental investigation has been conducted to study the effectiveness of film cooling on convective and radiative heat transfer at the stagnation point of a body traveling at hypersonic speeds. A simple, flat-faced cylinder has been selected as the model. A provision for attaching an optical fiber cable to collect radiation data was made near the center of the flat face. Thermocouples were strategically positioned along radial direction on the model's flat face to assess the convective heat transfer rates. An orifice, located at the center of the flat face, serves as the point for injecting coolant gas. Two different gases nitrogen and carbon dioxide, are used as coolant gases. Coolant gas injection, whether using carbon dioxide or nitrogen, resulted in reduced convective heat transfer rates compared to scenarios without coolant injection, with lighter gas offering superior cooling. The emission spectroscopy technique was utilized to study the radiation occurring at the stagnation point of the model. Radiation data showed emission lines arising from various contaminant species present in the shock tunnel facility.

Nomenclature

d_j = diameter of jet at exit plane

H = enthalpy

M_s = Mach number of incident shock

m_j = mass flow rate of the coolant jet

P_{0j} = total pressure of coolant jet

P_{0f} = pitot pressure

[1]*PhD scholar, Indian Institute of Technology Kanpur, jithins@iitk.ac.in*

[2] *PhD scholar, Indian Institute of Technology Kanpur, tkrishna@iitk.ac.in*

[3] *PhD scholar, Indian Institute of Technology Kanpur, nigotia.honhar@gmail.com*

[4]*Associate Professor, Indian Institute of Technology Kanpur, ibrahim@iitk.ac.in*

R_j = characteristic gas constant of coolant gas

T_{oj} =total temperature of the coolant jet

u = velocity

ρ = density

γ_j = ratio of specific heat values of the gaseous coolant

Subscripts

∞ = freestream conditions

w = wall conditions at 300K

o = reservoir conditions

1. Introduction

Reentry vehicles, such as spacecraft or capsules, reenter the Earth's or another planetary atmosphere typically at hypersonic speeds, leading to the formation of a bow shock ahead of the body. Across the bow shock, there is a significant rise in pressure and temperature. This increase is due to the conversion of the vehicle's kinetic energy into thermal energy. The extreme conditions across the bow shock cause the gases in the region to undergo dissociation and ionization. The dissociation and ionization processes, along with the high temperatures, expose the surface of the reentry vehicle to a significant amount of heat flux. This heat flux includes two main components, convective heat flux and radiative heat flux.

At reentry velocities, shock layer radiation can significantly contribute to the overall heat transfer to the surface of the reentry vehicle [1]. Studies indicate that for aeroassist trajectories with reentry velocities around 10 km/s, radiation can greatly impact the heat transfer to the vehicle's surface. In such scenarios, radiative heat transfer may exceed peak convective heat transfer by up to four times [2]. The extreme environmental conditions experienced during reentry can cause thermochemical damage to the vehicle's surface, presenting additional challenges. These challenges include issues with data and signal transmission between the vehicle and the ground, arising from the formation of ionized gas species in the shock layer ahead of the vehicle.

Thermal Protection Systems (TPS) serve to shield the surface of reentry vehicles from the extreme high-temperature conditions experienced during reentry. These systems are broadly classified into two categories: passive and active. Passive cooling involves harnessing natural heat dissipation mechanisms without the need for external devices or power sources, unlike active cooling methods. Ablative materials are commonly used in passive TPS, sacrificially absorbing and eroding under high

temperatures to dissipate heat away from the spacecraft. Thermal protection tiles, a type of insulation, exemplify such TPS components. Thermal Protection Systems (TPS) continue to confront difficulties despite their developments, such as material recession brought on by chemical reactions[3-4]. This recession can cause uncontrolled shape changes in the vehicle during flight, directly affecting its aerodynamic properties. To address recession, substantial safety margins are frequently integrated into the design, resulting in increased weight of the reentry vehicle. Hence, there is a necessity to investigate additional thermal protection mechanisms, either as alternatives or supplements to current TPS technology. Film cooling, an active cooling technique, is one such method.

Film cooling involves introducing a cooling fluid at specific points or multiple spots on a surface exposed to high temperatures to shield that surface from high heat fluxes. Various methods of injecting coolant have previously been examined, including techniques involving swirl ejection but it was found that a simple straight-out ejection provided the best results.[5]. Experiments have evaluated the efficacy of film cooling using a variety of coolant gases, and even liquid coolants [6]. Research has shown that film cooling has effectively reduced the rate of convective heat transfer from a hot gas stream to an exposed surface [7]. However, it can also act as a shield against thermal radiation if the injected coolant exhibits high radiation absorptivity. Carbon dioxide is recognized for its capacity to absorb specific forms of radiation, notably within the infrared (IR) segment of the electromagnetic spectrum, which is a fundamental aspect of the greenhouse effect. To date, no experiments have been conducted to assess the efficacy of film cooling in mitigating radiation effects occurring at the stagnation point of bodies traveling at hypersonic velocities. This paper focuses on this aspect. Different gases including nitrogen and carbon dioxide were chosen as the coolant gases and a comparison of their effectiveness in both convective and radiative heat transfer is being investigated in the current experimental campaign.

2. Experimental Setup

The experimental campaign was conducted using the shock tunnel of the Hypersonic Experimental Aerodynamics Laboratory, at the Indian Institute of Technology in Kanpur, India. Figure 1 shows the schematic of the facility. The driver and driven section are separated by the primary metal diaphragm. There are three PCB pressure sensors located on the driven section of the tube as shown in the figure, the signals from which are used to calculate the shock Mach number. A thin secondary diaphragm made of aluminium has been used as the secondary diaphragm instead of the conventionally used paper diaphragm. This is because the paper diaphragm tends to fragment into small particles upon its opening. These particles then mix with the freestream airflow, causing damage to both the model's surface and any sensors affixed to it upon impact.

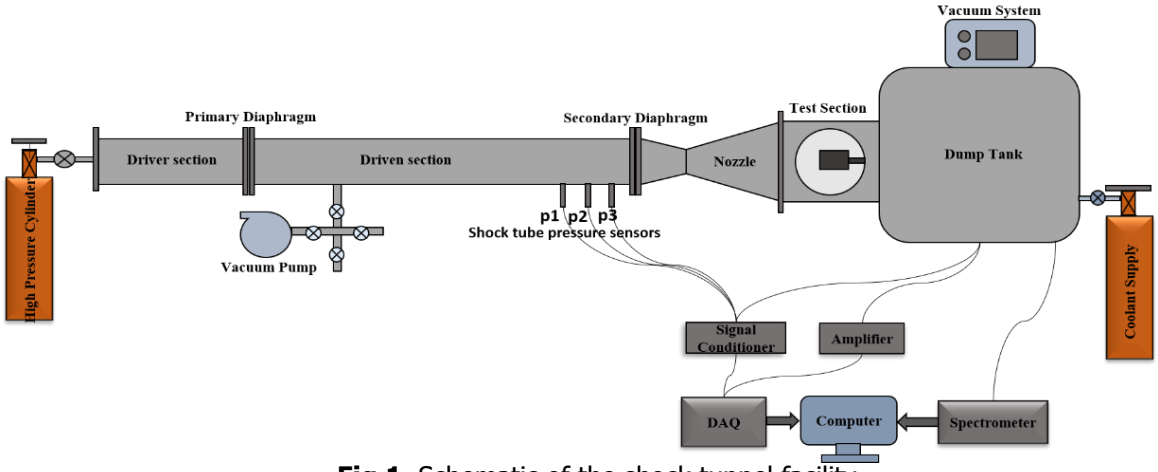

Fig 1. Schematic of the shock tunnel facility.

The model used here is a simple flat-faced cylindrical configuration having a diameter of 94mm. Figure 2 displays the photo of the test model. A 2mm orifice was made at the model's stagnation point through which the coolant gas will be supplied. Three in-house made E-type coaxial surface junction thermocouples have been strategically placed at distinct radial positions on the flat surface of the cylinder, specifically at distances of 10mm, 17mm, and 23mm from the model's stagnation point. An optical fiber cable with a quartz window has been securely positioned near the stagnation point within the provided setup. This optical fiber cable, in conjunction with an emission spectrometer, serves the purpose of capturing the radiation. Within the model, there exists a small plenum chamber designed to receive the supply of coolant gas from an external high-pressure gas cylinder during the experiment. There is a PCB pressure sensor flush mounted inside the plenum chamber which measures the total pressure of the coolant gas inside.

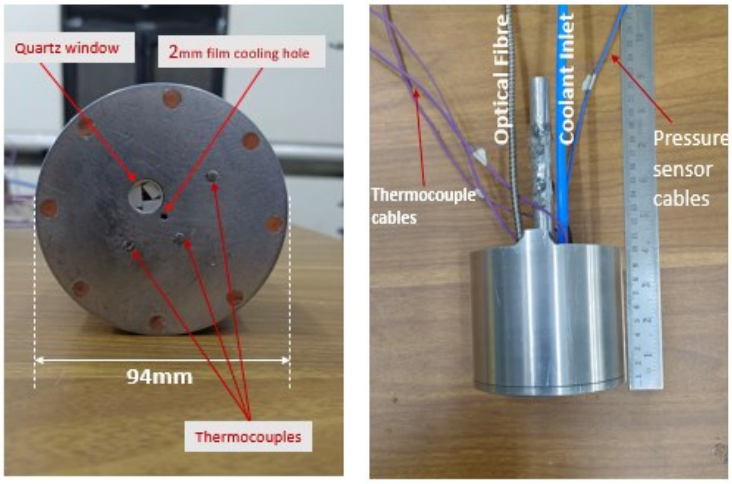

Fig 2. Image of the test model, showing the arrangement of thermocouple sensors and mounting of optical fiber cable.

For data acquisition during the experiments, the NI USB 6356 Multifunction I/O data acquisition device was utilized. A sampling rate of 1 million sampling/s per channel was selected for gathering pressure and temperature data. The data was collected for a period of 0.3 seconds after the trigger signal was obtained from the first shock tube pressure sensor (p_1). Radiation data was collected using the Ocean Optics USB4000, a compact fiber-optic spectrometer. The USB4000 can detect radiation across the UV-VIS-IR spectrum. The spectrometer was triggered using the shock tube pressure sensor, and an integration time of 4 milliseconds was employed. A Schlieren setup was employed for flow visualization. Chronos 1.4 high-speed camera and the Ocean Optics HPX-2000, 50Watts, Xenon Light source were used for the schlieren flow visualization, and the frame rate of the camera was set at 8000fps with an exposure time of 5micro seconds.

3. Results and Discussion

To determine the freestream conditions, pitot runs were conducted beforehand. The pitot pressure reading was measured to be around 29kPa, and a test duration of approximately 500 microseconds was recorded during the pitot runs. The GASEQ software was utilized to calculate the gamma value for the test gas under reservoir conditions at the nozzle inlet. This gamma value was subsequently employed in equations to determine freestream properties for an isentropic expansion process within the nozzle. NASA's Chemical Equilibrium with Applications (CEA) software was employed to compute the total enthalpy of the flow. The freestream conditions for the current experimental campaign are shown in Table 1.

Table 1. Test conditions and freestream properties.

Driven Gas	Air
Shock Mach number,M_s (±0.18)	4.6
Freestream Pressure,P_∞ (±60)	793Pa
Freestream Temperature,T_∞ (±28)	561K
Freestream Density,ρ_∞ (±0.002)	0.005kg/m^3
Freestream Velocity,u_∞ (±125)	2595 m/s
Total Pressure,P_{01}(±108)	1350kPa
Total Enthalpy,H_0 (±0.26)	2.68MJ/kg

Two distinct coolant gases, carbon dioxide(CO_2), and nitrogen(N_2), were individually employed for the current experimental campaign. Gases were fed from an external supply cylinder into the model's plenum chamber. The total pressure of the coolant gas (P_{0j}), as determined by the PCB sensor inside the plenum chamber must exceed the total pitot pressure(P_{0f}) in order for the coolant jet to successfully emerge through the film cooling orifice in opposition to the oncoming flow field. Figure 3 illustrates the pitot pressure signal alongside the total pressure signals of the coolant jets.

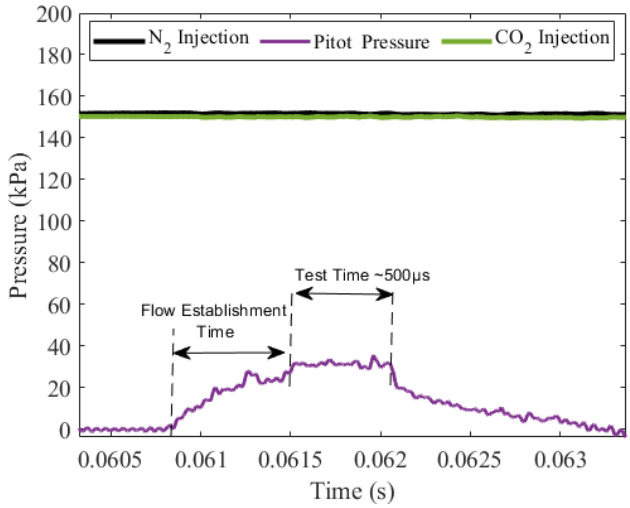

Fig 3. Pitot pressure signal and coolant jet total pressure signals for various coolants**.**

For the ongoing experiment, a pressure ratio, $P = \frac{P_{0j}}{P_{0f}}$ (the ratio of the coolant gas total pressure to pitot total pressure) of 5.1 was used for both the coolants, nitrogen and carbon dioxide. There exists a critical pressure ratio below which the coolant gas acts efficiently as a heat shield [8]. Once surpassing this critical threshold, the jet gains adequate momentum to disturb the bow shock formed ahead of the object. As a result, the bow shock distorts significantly in front of the model, leading to diminished effectiveness of the coolant gas as a heat shield.

3.1 Schlieren Visualization

The Schlieren images obtained in three different circumstances are shown in Figure 4. Figure 4a, which shows no coolant injection case, Figure 4b, coolant injection with nitrogen as coolant gas (P=5.1), and 4c, shows coolant injection with carbon dioxide as a coolant gas. Figures 4b and 4c demonstrate that both the coolant ejection has no discernible effect on the bow shock's structure, indicating that the selected pressure ratios are both well inside the critical pressure ratio's bounds.

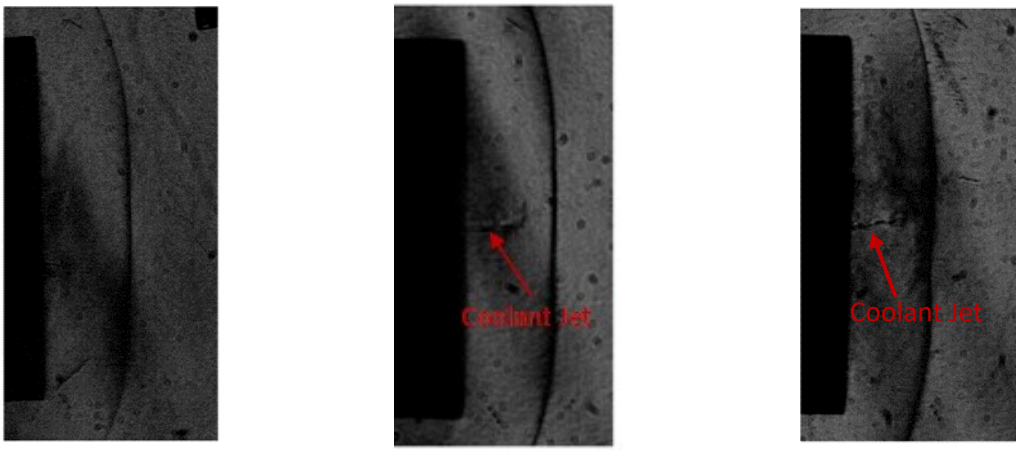

a, without coolant injection

b, with nitrogen injection

c, with carbon dioxide injection

Fig 4. Schlieren images during the test time for three different cases.

MATLAB Image Processing Toolbox was used to calculate the shock stand-off distances. Refer to Fig. 5 showing the shock standoff distances. A correlation was established between the known length, specifically the diameter of the cylinder, and the pixel count. This relationship was then used to determine the shock standoff distance at various locations.

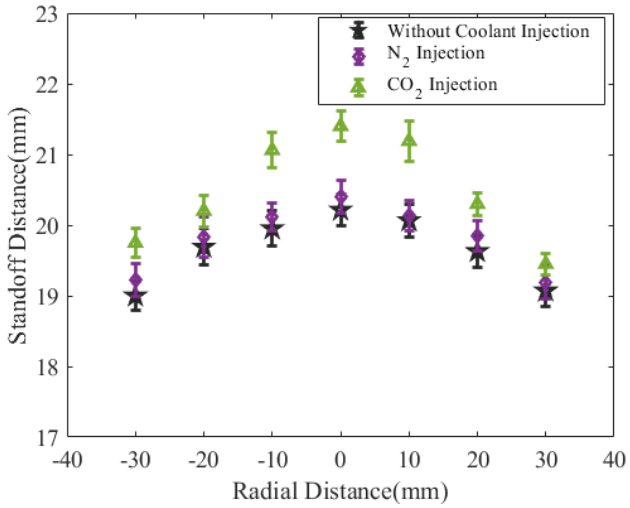

Fig 5. Shock stand-off distance along radial distance on the flat face of the model for three different cases.

The jet that is leaving is considered to be sonic since its total pressure is higher than the pitot total pressure [9]. The mass flow rate can therefore be determined using the chocked mass flow rate equation.

$$m_j = \left(\frac{P_{oj}}{\sqrt{T_{oj}}}\right)\left(\frac{\pi}{4}d_j^2\right)\sqrt{\frac{\gamma_j}{R_j}\left(\frac{2}{\gamma_j+1}\right)^{\frac{\gamma_j+1}{\gamma_j-1}}} \quad (1)$$

The coolant gas is delivered from an external cylinder to the plenum chamber of the test model inside the tunnel. The total temperature (T_{oj}) is determined by assuming an isentropic expansion originating from the external supply cylinder of gas. The characteristics of the coolant gases are detailed in Table2.

Table 2. Coolant gas properties.

Coolant	P_{oj} (kPa)	T_{oj} (K)	γ_j	m_j (kg/s)
Nitrogen	150	272	1.4	$1.13*10^{-3}$
Carbon dioxide	150	278	1.3	$1.37*10^{-3}$

3.2 Heat Transfer Assessment

Thermocouples were employed to measure convective heat transfer rates. Three thermocouples, situated at radial distances of 10 mm, 17 mm, and 23 mm from the model's stagnation point, recorded the transient surface temperature history during the test period. The heat flux values are derived from the measured temperature changes based on unsteady one dimensional heat conduction theory [10-12]. For instance, Figure 6a presents temperature signals acquired at the 10mm radial position for a specific case with P=5.1, nitrogen coolant injection. Corresponding to the rising temperature signal, Figure 6b displays the convective heat transfer rate during the test period.

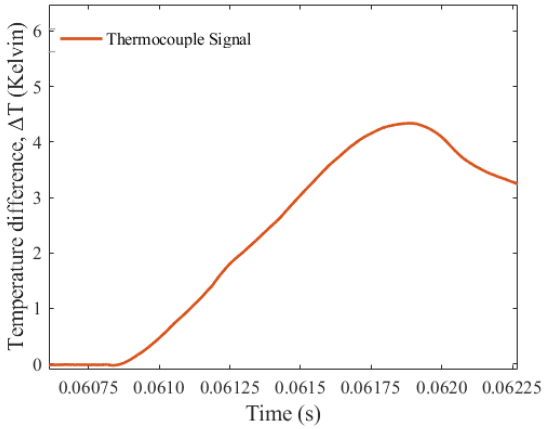

a, Temperature signal recorded by the thermocouple at 10mm radial distance.

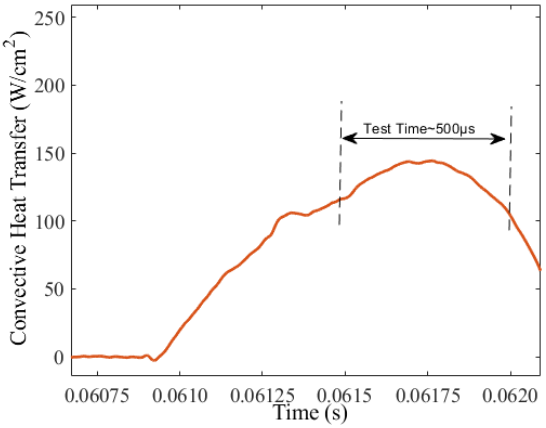

b, Heat transfer plot obtained from thermocouple at 10mm radial distance

Fig. 6 Temperature signal recorded by the thermocouple at 10mm radial distance and the corresponding heat transfer plot, for a run with nitrogen coolant injection.

Figure 7 illustrates the average convective heat flux values for each radial location over the test duration for three scenarios: one with nitrogen as a coolant, one with carbon dioxide as a coolant, and one without any coolant injection. For the case without coolant injection, the convective heat flux value shows a greater magnitude closer to the stagnation point of the body. The shock's strength is greatest near the center or stagnation point as it presents itself as a normal shock in this specific area. This results in extensive compression within the flow, leading to considerable increases in both pressure and temperature within this region. Towards the outer edges of the bow shock, its strength gradually weakens. Additionally, as we move radially outward from the central stagnation point, the flow velocity gradually increases, causing the flow to expand. This leads to a decrease in both pressure and temperature, resulting in a reduction in the experienced heat flux along this direction.

It is evident that there is a decrease in heat transfer observed for both cases utilizing nitrogen and carbon dioxide as cooling gases. The heat flux values have experienced a more pronounced decrease with nitrogen as the coolant gas compared to carbon dioxide across nearly all locations in the system. Because nitrogen possesses a higher specific heat capacity than carbon dioxide, it can absorb and carry away more heat energy, consequently leading to a decrease in heat flux.

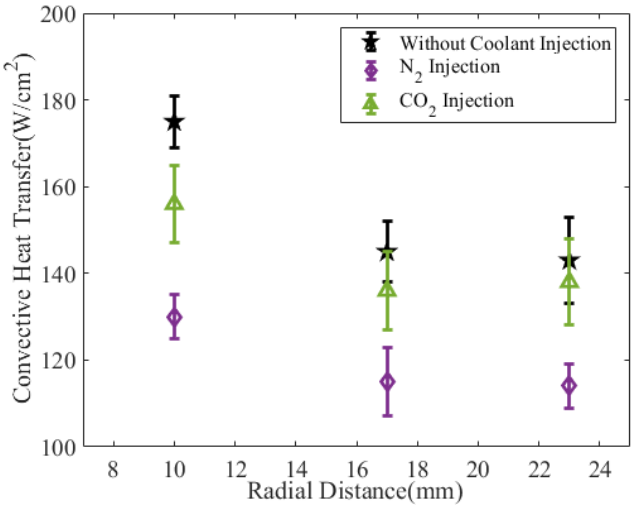

Fig 7. Average convective heat transfer values over radial positions along the model's flat face.

Figure 8 illustrates plots depicting the percentage reduction in heat transfer rate across the radial direction. It can be seen that nitrogen gas exhibits superior cooling performance at locations farther from the injection point compared to carbon dioxide. At the 10mm radial location, a maximum reduction of approximately 25% is observed for the nitrogen coolant case, followed by reductions of 21% at the 17mm location and 20% at the 23mm location, respectively. Likewise, in the case of carbon dioxide coolant, the maximum reduction of around 10% is observed near the stagnation region at a radial distance of 10mm. This is followed by reductions of 6% at the 17mm location and 4% at the 23mm radial location.

It can be seen that nitrogen gas exhibits superior cooling performance at locations farther from the injection point compared to carbon dioxide. Lighter gases diffuse more readily through a fluid medium compared to heavier gases. This enhances their ability to mix and spread out along a surface, contributing to their rapid expansion downstream, consequently offering more effective cooling at locations farther from the injection point compared to a heavier gas.

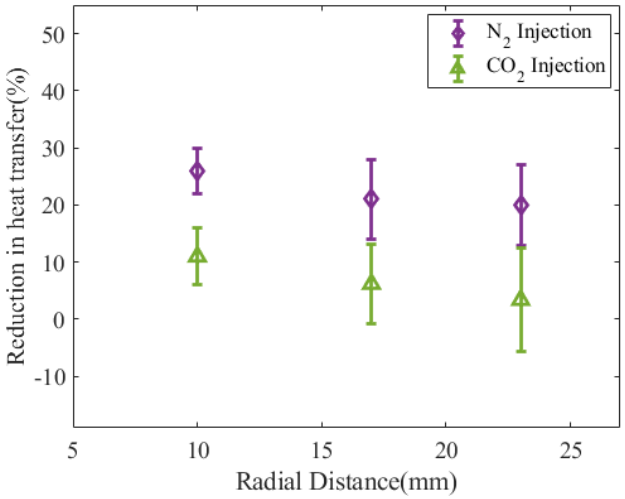

Fig 8. Percentage reduction in convective heat transfer rates at different radial locations for cases with coolant injection.

3.3 Radiation Measurements

During the course of the experiments, a glow, was detected through the test window. To investigate and analyze this radiant emission more closely, a spectrometer was employed. As a result, the data pertaining to radiation was recorded. Figure 9 displays the spectrum for the run without any coolant injection, revealing distinct peaks at various wavelengths.

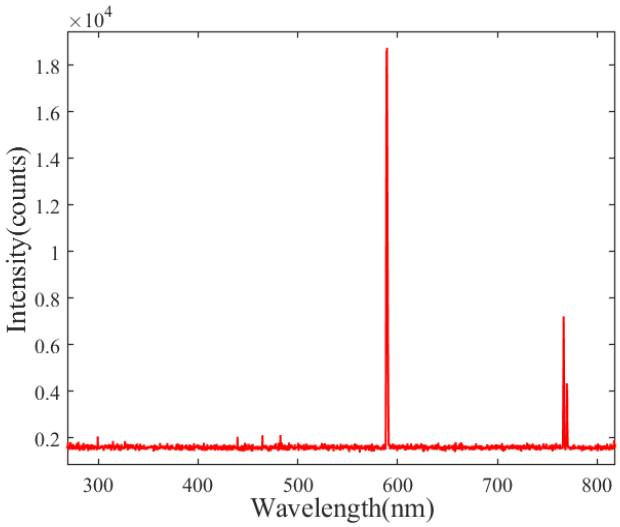

Fig 9. Emission Spectrum for run without coolant injection showing distinct peaks at different wavelengths.

By utilizing the NIST database, relevant literature sources, and the Spectrum Analyzer software[14-15], the species linked to the spectral lines were successfully identified. Figure 9 shows the spectrum captured for a run without any coolant injection.

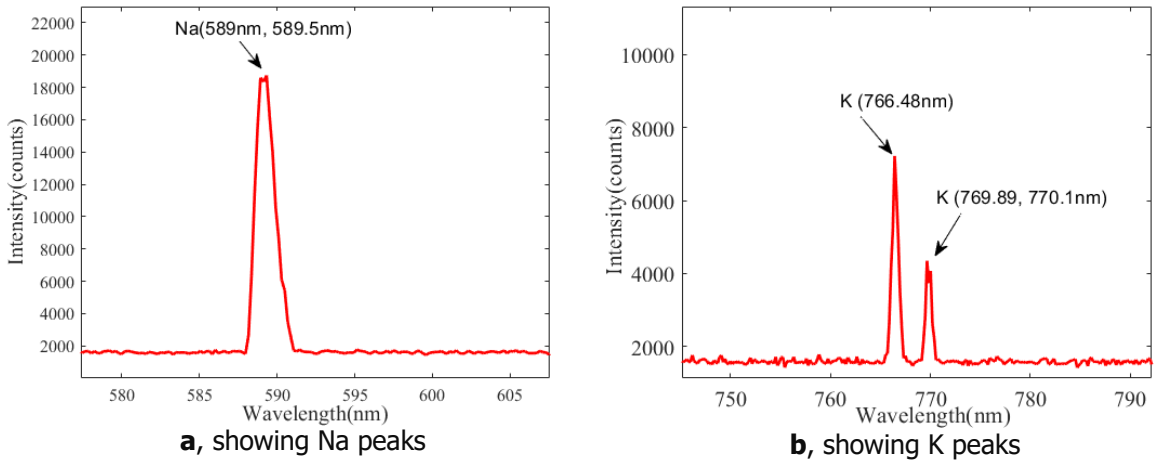

a, showing Na peaks

b, showing K peaks

Fig 10. Emission Spectrum showing various elements that are contributing to the radiation.

Figure 10 provides a magnified representation of each line depicted in Figure 9, facilitating the identification of each observed peak. Figure 10a shows one of the most prominent peaks observed in the spectrum. It was determined that the emission lines at 589.4 nm and 589.5 nm were caused by the electronic excitation of (Na I) sodium [15-16]. They are so close that they have almost merged together. The presence of sodium radiation can be attributed to the inherent existence of sodium chloride in the atmosphere [17-19].Figure 10b shows the lines due to potassium (K I) at 766.48nm,769.89nm, and 770.1nm. The presence of potassium can be linked to the utilization of grease in various areas of the facility. The radiation must have been affected by any grease that may have been combined with the gas inside the shock tube [20].

Figure 11 depicts a comparison of the spectra for different runs, including those with and without coolant injection.

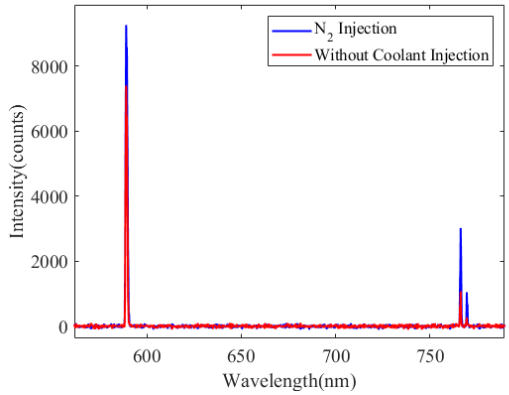

a, Spectrum showing higher radiation intensity with N_2 injection compared to without coolant.

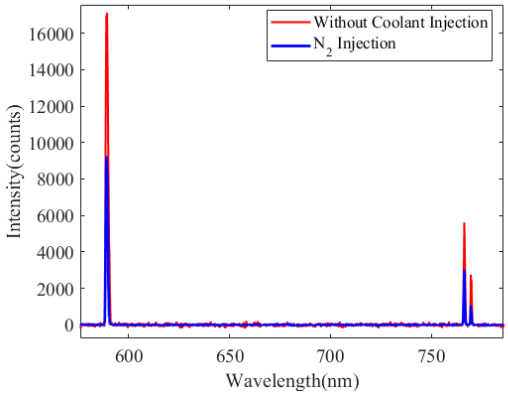

b, Spectrum showing higher radiation intensity for without coolant case compared to N_2 injection case.

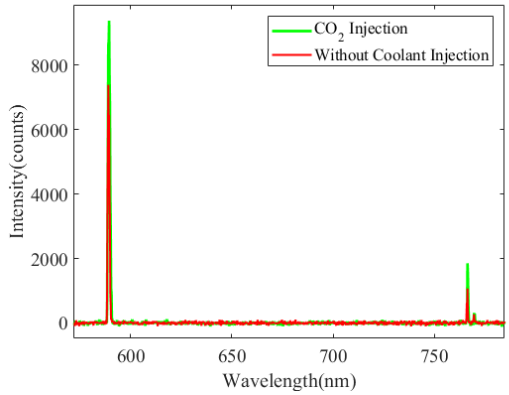

c, Spectrum showing higher radiation intensity with CO_2 injection compared to without coolant.

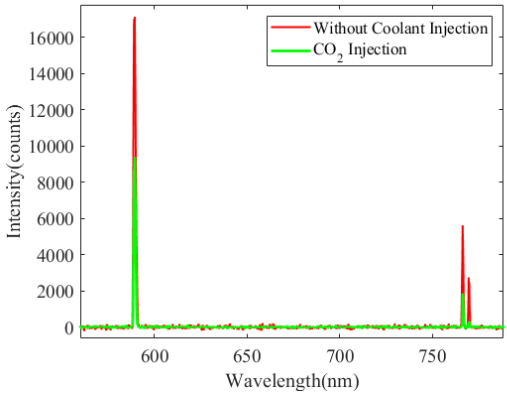

d, Spectrum showing higher radiation intensity for without coolant case compared to CO_2 injection case.

Fig. 11 Comparision of the spectrum for different runs involving with and without coolant injection.

Since the quantity of contaminants in each run is random, uncontrollable, or unpredictable, the radiation intensity also fluctuates. In Figures 11a and 11c, the radiation intensity appears higher for cases with coolant injection, whereas in Figures11b and 11d, it is higher for cases without coolant injection. These observations align with the idea that radiation is induced by the presence of contaminants. Thus the experiments clearly demonstrate that the observed glow was the radiation from the impurities and not the test gas, as the enthalpy levels are not high enough to cause air radiation.

4. Conclusion

Experiments were carried out in a shock tunnel operating at an enthalpy of 2.68 MJ/kg to examine the impact of film cooling on both convective and radiative heat transfer in hypersonic flows. A simple flat cylinder was used as the model for the current study and experiments are conducted at zero zero-degree angle of attack. Nitrogen and carbon dioxide are used as the coolant gases. These gases are introduced through a 2mm orifice located at the stagnation point of a flat cylindrical model. Thermocouples were used to evaluate the convective heat transfer rate. Radiation data was captured using a spectrometer.

- The implementation of coolant injection, utilizing both nitrogen and carbon dioxide, results in a decrease in convective heat transfer rates, thereby confirming their effectiveness as coolant gases in reducing convective heat flux.
- Nitrogen exhibited superior performance as a coolant compared to carbon dioxide due to its properties such as low molecular weight and higher specific heat capacity. These characteristics enable nitrogen to effectively carry away more heat from various downstream locations.
- In the spectrum obtained, various contaminant species like sodium and potassium are observed to be contributing to the radiation. Due to their uncontrollable and random inclusion as contaminants in the flow field, no significant conclusion could be reached on the effect of film cooling on radiation heat transfer measurements.

References

1. Grinstead, J.H., Wright, M.J., Bogdanoff, D.W. and Allen, G.A.: Shock radiation measurements for Mars aerocapture radiative heating analysis. Journal of Thermophysics and Heat Transfer, 23(2) pp.249-255 (2009). https://doi.org/10.2514/1.37281

2. Jacobs, C.M., McIntyre, T.J., Morgan, R.G., Brandis, A.M. and Laux, C.O.: Radiative heat transfer measurements in low-density titan atmospheres. Journal of Thermophysics and Heat Transfer, 29(4), pp.835-844 (2015). https://doi.org/10.2514/1.T4519

3. Laub, B. and Venkatapathy, E.: Thermal protection system technology and facility needs for demanding future planetary missions. In planetary probe atmospheric entry and descent trajectory analysis and science , Vol. 544, pp. 239-247 (2004).

4. Ewenz Rocher, M., Hermann, T. and McGilvray, M.: Oxidation Response of Transpiration-Cooled ZrB 2 on a Hypersonic Stagnation Point. Journal of Spacecraft and Rockets 59.5, pp. 1486-1495 (2022).https://doi.org/10.2514/1.A35309

5. Warren, C.H.E.: An experimental investigation of the effect of ejecting a coolant gas at the nose of a bluff body. Journal of Fluid Mechanics, 8(3), pp.400-417 (1960).

6. Yuan, C., Li, J., Jiang, Z. and Yu, H.: Experimental investigation of liquid film cooling in hypersonic flow. Physics of Fluids, 31(4), p.046101 (2019).

7. Sahoo, N., Kulkarni, V., Saravanan, S., Jagadeesh, G. and Reddy, K.P.J.: Film cooling effectiveness on a large angle blunt cone flying at hypersonic speed. Physics of Fluids, 17(3), p.036102 (2005).

8. Finley, P.J.: The flow of a jet from a body opposing a supersonic free stream. Journal of Fluid Mechanics, 26(2), pp.337-368 (1966). doi:10.1017/S0022112066001277

9. Ibrahim, S.M., Sriram, R. and Reddy, K.P.J.: Experimental investigation of heat flux mitigation during Martian entry by coolant injection, Journal of Spacecraft and Rockets, 51(4), pp.1363-1368 (2014). https://doi.org/10.2514/1.A32846

10. Rout, A.K., Sahoo, N. and Kalita, P.: Transient Response Characteristics and Performance Assessment of a Calorimetric Surface Junction Probe Under Impulsive Thermal Loading. Journal of Heat Transfer, 143(6) (2021).

11. Mohammed, H., Salleh, H. and Yusoff, M.Z.: Design and fabrication of coaxial surface junction thermocouples for transient heat transfer measurements. International Communications in Heat and Mass Transfer, 35(7), pp.853-859 (2008).

12. Desikan, S.L.N., Suresh, K., Srinivasan, K. and Raveendran, P.G.: Fast response co-axial thermocouple for short duration impulse facilities. Applied Thermal Engineering 96, 48-56 (2016). https://doi.org/10.1016/j.applthermaleng.2015.11.074

13. Cook, W.J and Felderman, E.J.: Reduction of Data from Thin Film Heat Transfer Gauges. A Concise Numerical Technique. AIAA Journal, Vol.4, No.3, pp 561-562 (1996). https://doi.org/10.2514/3.3486

14. Navrátil, Z., Trunec, D., Šmíd, R. and Lazar, L.: A software for optical emission spectroscopy-problem formulation and application to plasma diagnostics. Czechoslovak Journal of Physics, 56, pp.B944-B951 (2006).

15. NIST Atomic Spectra Database (ver. 5.10), https://physics.nist.gov/asd, National Institute of Standards and Technology, Gaithersburg, MD. https://doi.org/10.18434/T4W30F

16. Saranyamol, V.S.: Effect of shock strength on the radiation of focusing shock wave. European Journal of Mechanics-B/Fluids, 97, pp.128-135 (2023). https://doi.org/10.1016/j.euromechflu.2022.10.001

17. Nomura, S., Takayanagi, H., Fujita, K., Tanno, H., Komuro, T. and Itoh, K.: Spectroscopic investigation on anomalous heating in free piston shock tunnel HIEST. In 11th AIAA/ASME Joint Thermophysics and Heat Transfer Conference , p. 2545 (2014). https://doi.org/10.2514/6.2014-2545

18. Sharma, S.P. and Park, C.: Operating characteristics of a 60-and 10-cm electric arc-driven shock tube. I-The driver. II-The driven section. Journal of Thermophysics and Heat Transfer, 4(3), pp.259-265 (1990).

19. Codron, D.A., Cruden, B.A. and Ho, T.: Emission spectroscopy characterization of thermal protection system materials in arc-heated flows. In 45th AIAA Plasmadynamics and Lasers Conference, p. 2112 (2014). https://doi.org/10.2514/6.2014-2112

20. Anbuselvan, K.K.N., Anand, V., Krishna, Y. and Rao, M.G.: Spectroscopic investigations on impurities and their effect on the electron number density in the shock tube. Journal of Quantitative Spectroscopy and Radiative Transfer, 272, p.107744 (2021).